

Lewis Grasso

*Cooperative Institute for Research in the Atmosphere, Colorado State University, Fort Collins, Colorado*

Daniel T. Lindsey

*NOAA/NESDIS, Fort Collins, Colorado*

## 1. INTRODUCTION

First efforts to simulate thunderstorms used an idealized framework with horizontal domains about 100 km on a side and horizontal grid spacings of 1 to 2 km. Further, the initial domain was horizontally homogeneous. A warm bubble was then used to trigger a single storm for study. Today, computer capabilities allow for more detailed simulations. We have initialized the CSU-RAMS model with observations from 8 May 2003. With multiple, non-moving nested grids, a right-moving storm was captured within the fourth grid. This grid was about 400 km on a side and had horizontal grid spacing of 400 m. With relatively small horizontal grid spacings, we have an opportunity to study the evolution of a hook echo that developed. This can help our understanding of the role of storm rotation and falling hydrometeors in the development of the hook appendage. Further, the development of both a warm rear flank downdraft and other warm regions within the downdraft can be examined. Even though 400 m is too large to resolve a tornado, closed surface rotation exists in the expected position for tornado development. We will show the evolution of the hook echo, warm rear flank downdraft, and surface rotation of this storm. In addition, a synthetic polar orbiting satellite image at 11.02  $\mu\text{m}$  of the storms in grid 4 will be shown.

## 2. RAMS OVERVIEW

The numerical cloud model used for this study was RAMS43 (Pielke et al. 1992). The following features of RAMS were used to simulate the mesoscale weather events:

- The model was run non-hydrostatically and compressible (Tripoli and Cotton 1982).
- Momentum was advanced using a leapfrog scheme while scalars were advanced using a forward scheme. Both methods used second order advection.
- Vertical and horizontal turbulence coefficients were parameterized using the Smagorinsky (1963) deformation based eddy viscosity with stability modifications (Lilly 1962).
- Hydrometeors were predicted with a two-moment bulk microphysical scheme (Meyers et al. 1997). Mass mixing ratio and number concentration were prognosed for six of the seven hydrometeor types while the mean diameter was diagnosed. Cloud droplet mass mixing ratio, however, was predicted using a one-moment scheme. (Work is ongoing to include cloud droplets into the two-moment scheme.) The following hydrometeor species were included in the simulation: Cloud droplets, rain droplets, aggregates, graupel, hail, snow, and pristine ice. Both graupel and hail are mixed phased; that

- is, liquid water may exist on the surface of each particle. Snow and pristine ice are each divided into five habit categories: Columns, hexagonal, dendrites, needles, and rosetta.
- Other prognostic variables were the three components of velocity— $u$ ,  $v$ ,  $w$ ; perturbation Exner function,  $\pi^*$ ; total water,  $r_{\{t\}}$ ; and ice-liquid potential temperature,  $\theta_{\{il\}}$  (Tripoli and Cotton 1981).
- RAMS uses the Arakawa fully staggered C grid (Arakawa and Lamb 1981).
- Perturbation Exner function tendencies, used to update the momentum variables, were computed using a time split scheme—similar to Klemp and Wilhelmson (1978).
- Lateral boundaries used the Klemp-Wilhelmson condition; that is, the normal velocity component specified at the lateral boundary is effectively advected from the interior.
- A wall with friction layers was specified at the top boundary.
- Land Ecosystem Atmospheric Feedback model, version 2 (LEAF2) (Walko et al. 2000) was employed.

## 3. RESULTS

Figure 1 shows a synthetic NPOESS image of the simulated severe weather event over eastern Kansas at 11.02  $\mu\text{m}$ . The storm of interest is depicted by the eastern most cold top to the right of center. Surface ground relative wind vectors and contours of virtual potential temperatures are shown with the precipitation field near 1400 m in the sequence of panels in Fig. 2. This figure reveals the development of the hook echo at a temporal frequency of five minutes from 1835 to 1900 UTC. Ground relative winds in excess of 25 m s are denoted by red vectors. Therefore, this storm may be classified as being severe. In addition to a hook echo, a warm rear flank downdraft was also captured by the simulation. Figure 3 shows virtual potential temperature—colored—on the lowest six model levels at 1900 UTC. Just below 700 m, the largest values of virtual potential temperature—associated with the storm—were co-located with the rear flank downdraft.

A trajectory model was developed to provide guidance as to the source of precipitation within the hook. Further, the model was also used to inquire about the source of air within the warm rear flank downdraft. Trajectories were calculated from a fourth order Runge-Kutta procedure. RAMS data was saved every five minutes. Trajectories were advanced with a five second timestep. RAMS output was linearly interpolated in each of the three spatial directions and in time to each particle. A total of 10,000 particles were used to track particles within the hook while 5050 particles were used in the triangular region within the rear flank downdraft. Although trajectories were run backwards in time from 1900 to 1845 UTC, results will be presented forward in time from 1845 (6300 s) to 1900 UTC (7200 s).

Figure 4 shows the evolution of 10,000 particles that were placed at the base of the hook echo near 1400 m. If the precipitation condensate—cloud water was not considered precipitation—exceeded 1 g kg then any particle in this environment was given a fall speed of 1 m s. Results suggest that some of the particles passed through the forward flank of the storm while being lifted from 6300 s to 6800 s. From 6800 s to 7200 s, particles entered the updraft from the right flank and ascended relatively rapidly before exiting the updraft and sinking back into the base of the hook appendage. In order to test the sensitivity of precipitation fall speed, this run was repeated with no adjustment to particle fall speed based on precipitation amount. That is, the fall speed was set to zero. The evolution of the particles is shown in Fig. 5. Results from this run are similar to those shown in Fig. 4.

A triangular region was used to initialize 5050 particles in the warm rear flank region of the storm near 700 m (Fig. 6). Results suggest that air from two different regions of the storm end up in the warm rear flank downdraft. One region is the forward flank of the storm. These particles move from the forward flank to the rear flank of the storm. The second region is near surface air on the right rear flank. These particles rise up and over the rear flank gustfront, turn anticyclonically and move towards the storm, and finally enter the rear flank downdraft.

#### 4. FUTURE DIRECTION

In the future, additional trajectories will be run to examine sensitivities to the initial location of particles. That is, the initial particle locations will be shifted vertically and horizontally.

#### References:

Arakawa, A., and V. Lamb, 1981: A potential enstrophy and energy conserving scheme for the shallow water equations. *Mon. Wea. Rev.*, **109**, 18-36.

Klemp, J. B. and R. B. Wilhelmson, 1978: The simulation of three-dimensional convective storm dynamics. *J. Atmos. Sci.*, **35**, 1070-1096.

Lilly, D. K., 1962: On the numerical simulation of buoyant convection. *Tellus*, **14**, 148-172.

Meyers, M. P., R. L. Walko, J. Y. Harrington, and W. R. Cotton, 1997: New RAMS cloud microphysics parameterization. Part II: The two-moment scheme. *Atmos. Res.*, **45**, 3-39.

Pielke, R. A., W. R. Cotton, R. L. Walko, C. J. Tremback, W. A. Lyons, L. D. Grasso, M. E. Nicholls, M. D. Moran, D. A. Wesley, T. J. Lee, J. H. Copeland, 1992: A comprehensive meteorological modeling system-RAMS. *Meteor. and Atmos. Phys.*, **49**, 69-91.

Smagorinsky, J., 1963: General circulation experiments with the primitive equations. Part 1: The basic experiment. *Mon. Wea. Rev.*, **91**, 99-164

Tripoli, G. J., and W. R. Cotton, 1981: The use of ice-liquid water potential temperature as a thermodynamic variable in deep atmospheric models. *Mon. Wea. Rev.*, **109**, 1094-1102.

Tripoli, G. J., and W. R. Cotton, 1982: The Colorado State University three dimensional cloud mesoscale model, 1982. Part I: General theoretical framework and sensitivity experiments. *J. Rech. Atmos.*, **16**, 185-220.

Walko, Robert L., L. E. Band, J. Baron, T. Kittel, G. F., R. Lammers, T. J. Lee, D. Ojima, R. A. Pielke, C. Taylor, C. Tague, C. J. Tremback, P. L. Vidale, 2000: Coupled Atmosphere-Biophysics-Hydrology Models for Environmental Modeling. *J. Appl. Meteor.*, **39**, 931-944.

Acknowledgments: This material is based on work supported by the National Oceanic and Atmospheric Administration under Grant NA67RJ0152. The views, opinions, and findings in this report are those of the authors and should not be construed as an official NOAA and or U.S. Government position, policy, or decision.

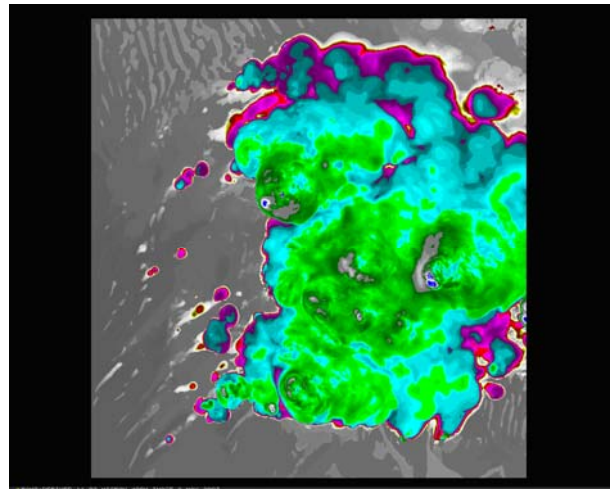


Figure 1: Synthetic NPOESS 11.02  $\mu\text{m}$  image of the 8 May 2003 simulation in grid 4.

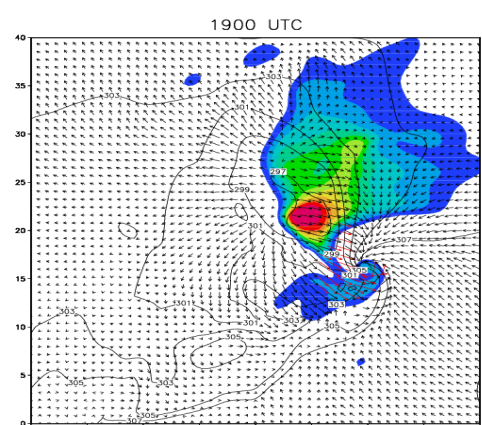
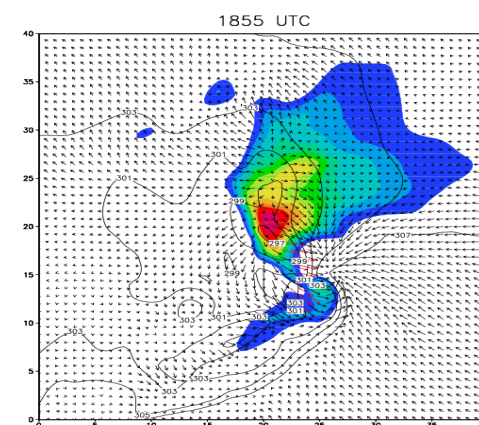
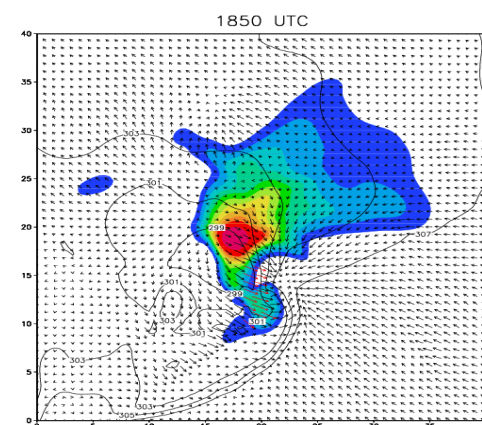
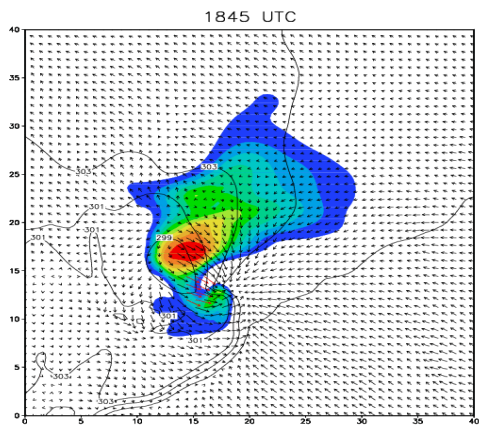
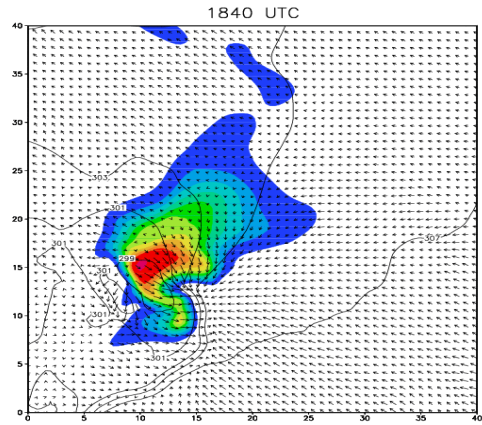
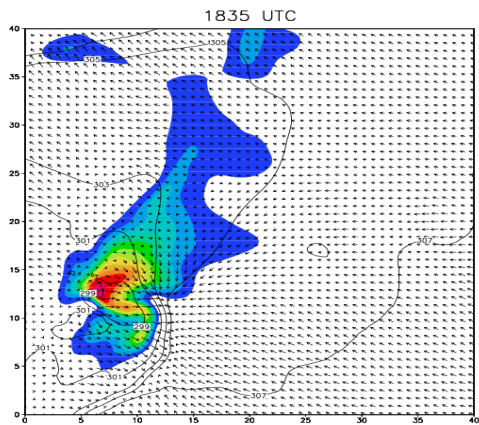


Figure 2: Temporal evolution of the hook echo. Precipitation at 1400 m is colored. Near surface ground relative wind and virtual potential temperature are also shown. Winds exceeding 25 m s are colored red.

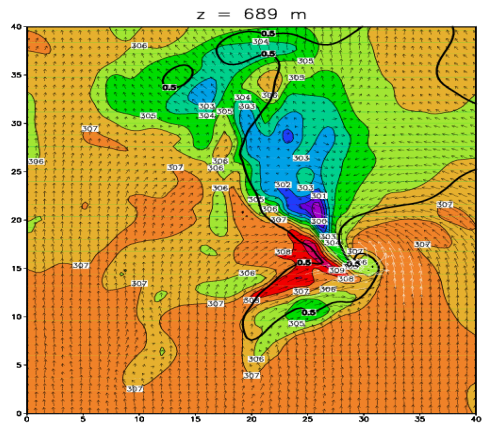
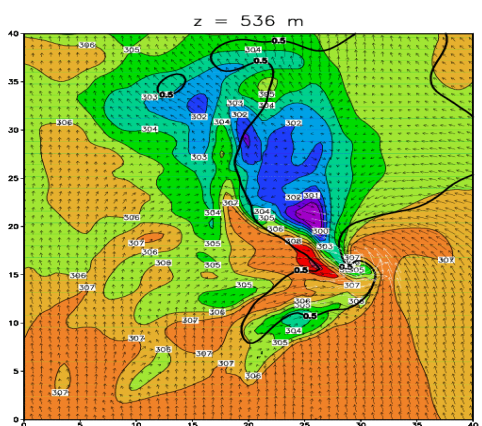
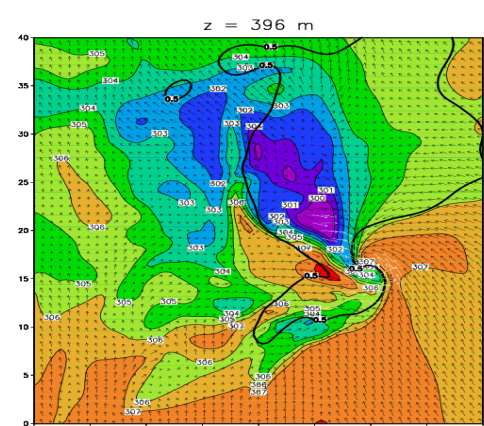
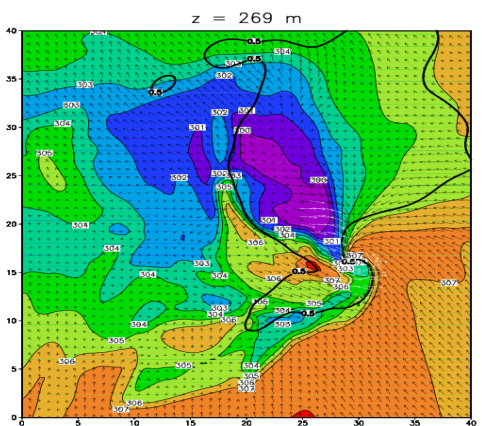
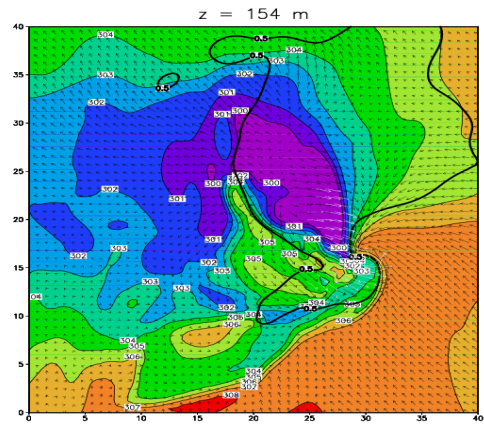
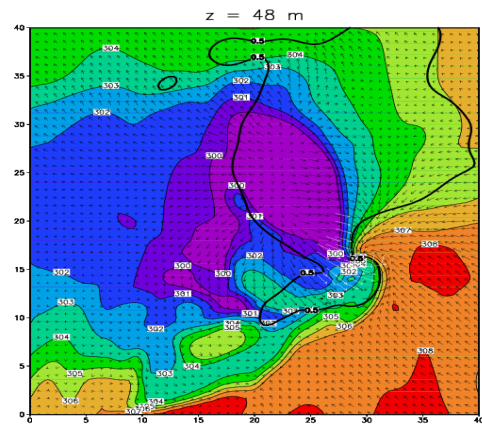
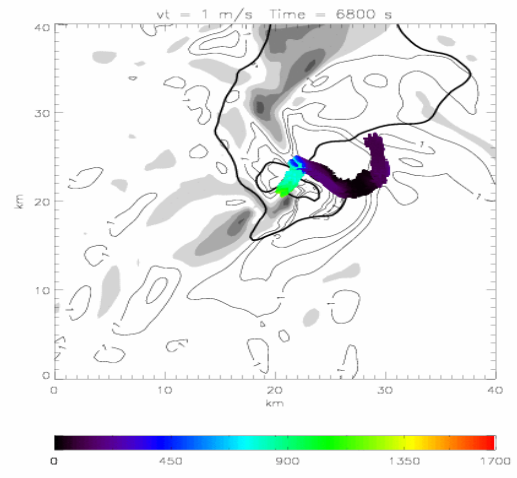
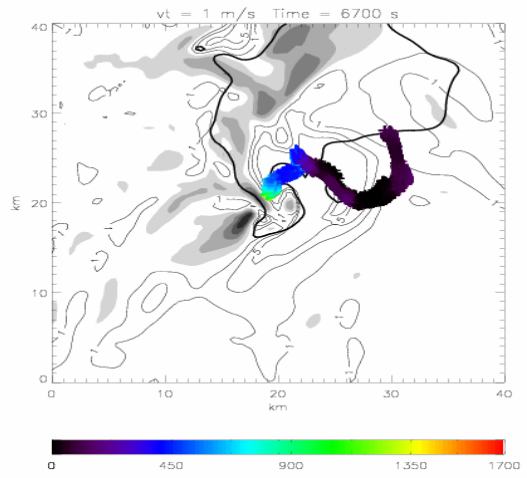
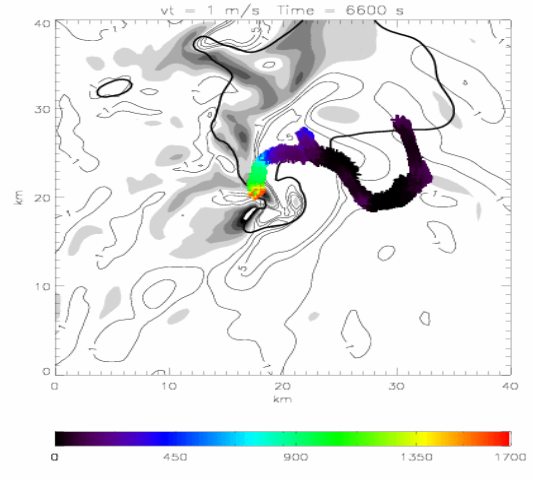
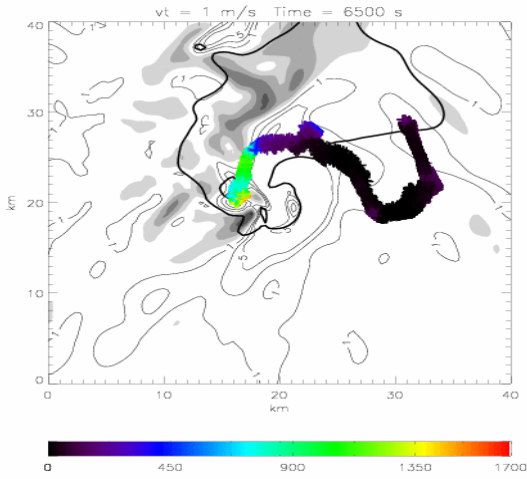
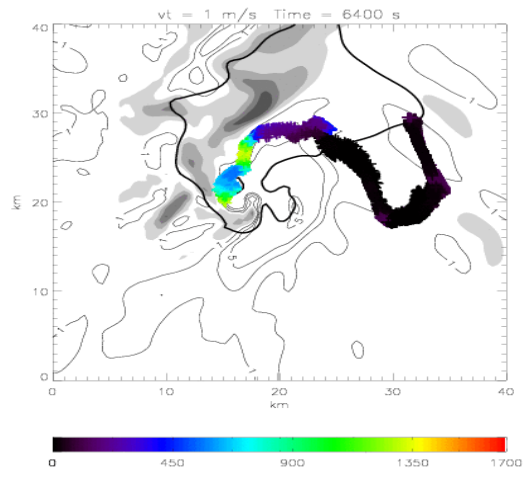
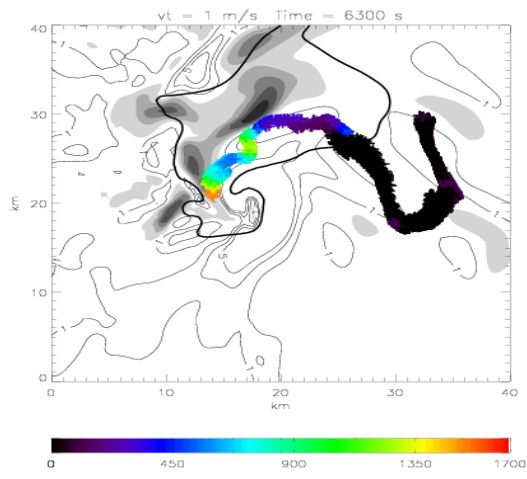


Figure 3: Virtual potential temperature—colored—in the lowest six model levels at 1900 UTC. The outline of the precipitation is denoted by the thick black contour. Ground relative winds at each level are also shown. Winds in excess of 25 m s are white



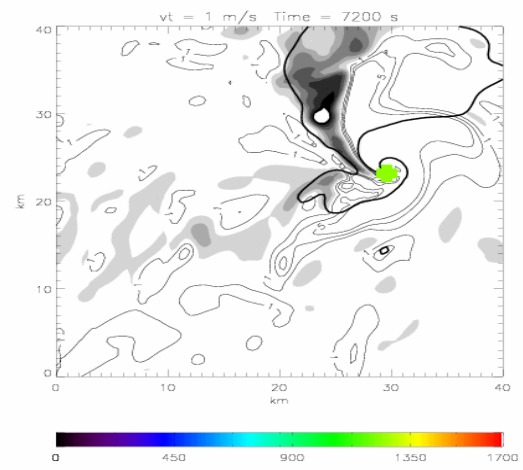
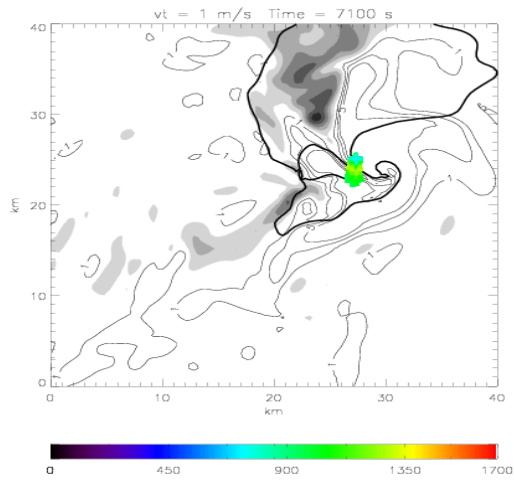
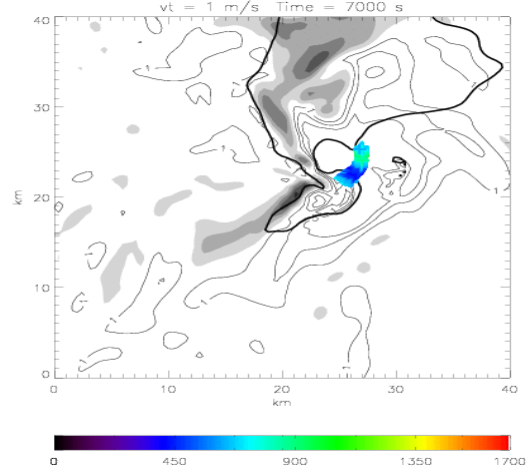
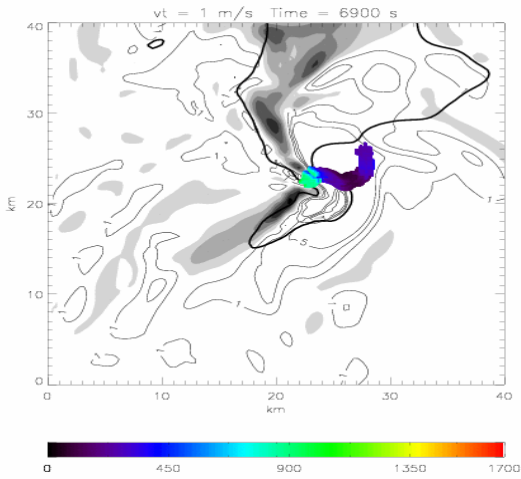
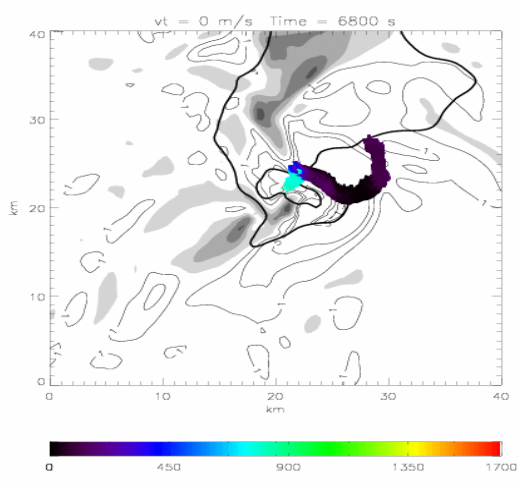
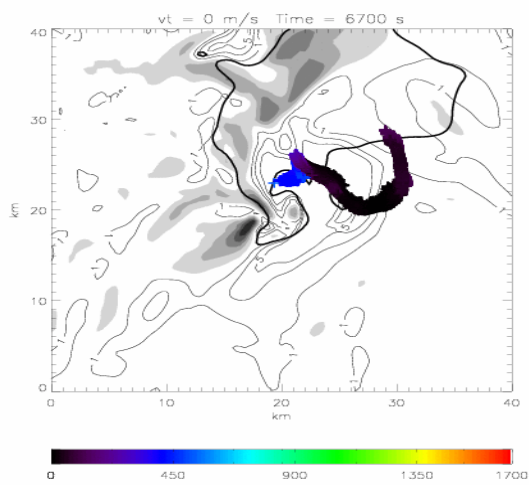
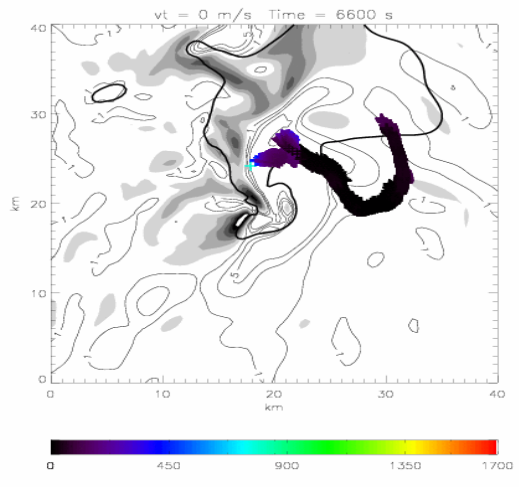
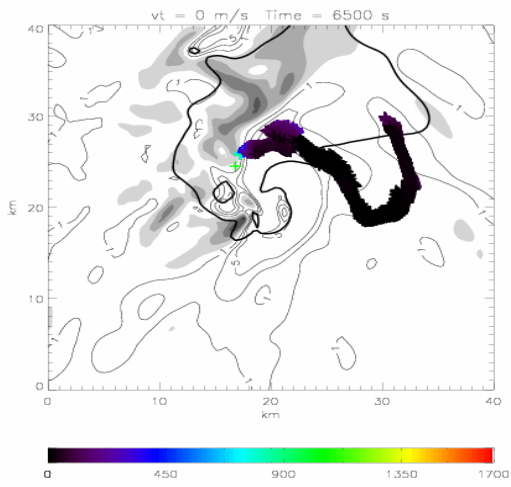
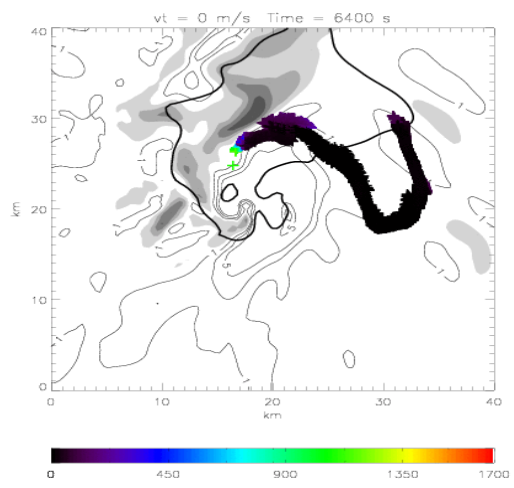
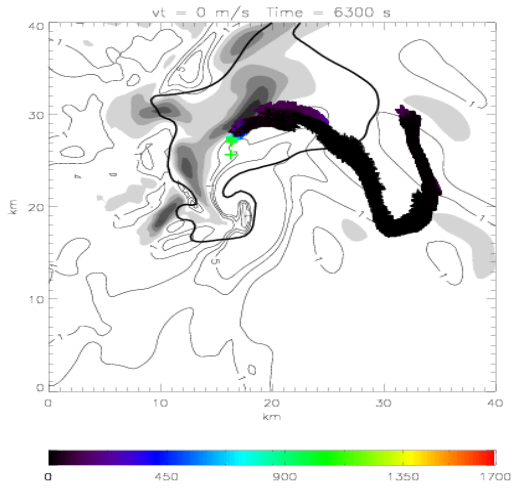


Figure 4: Time series of 10,000 particles initialized at the base of the hook appendage near 1400 m. Particle positions are shown every 100 s. Precipitation is outlined by the thick contour. Downdraft is grey shaded while updraft is denoted by thin contours. Particle terminal fall speeds are set to 1 m s while in precipitation, otherwise terminal fall speeds are zero. Particle height is indicated by the color bar below each panel.



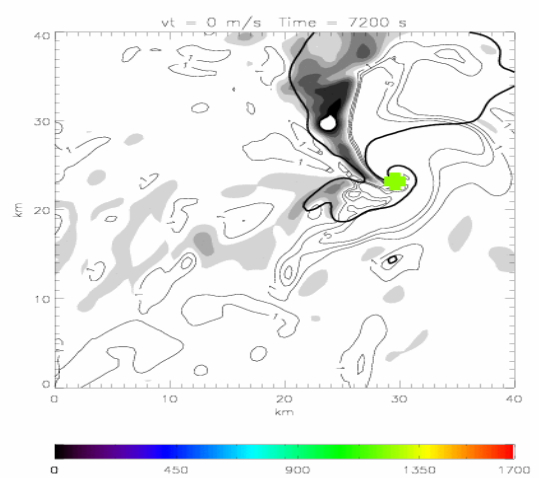
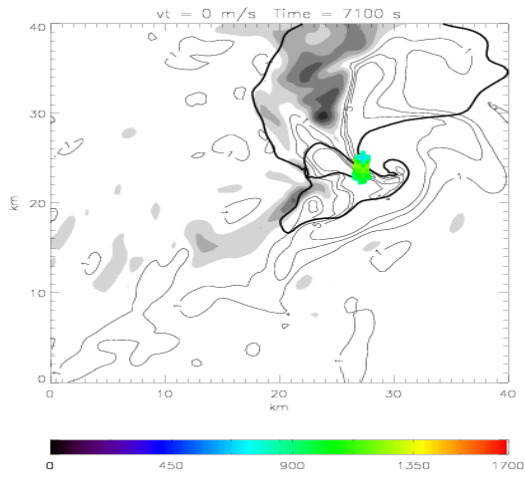
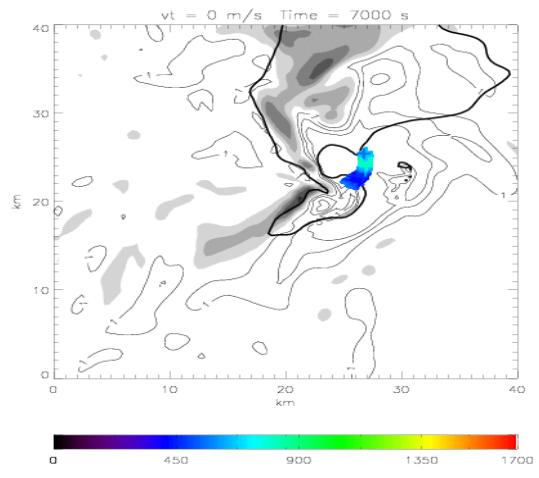
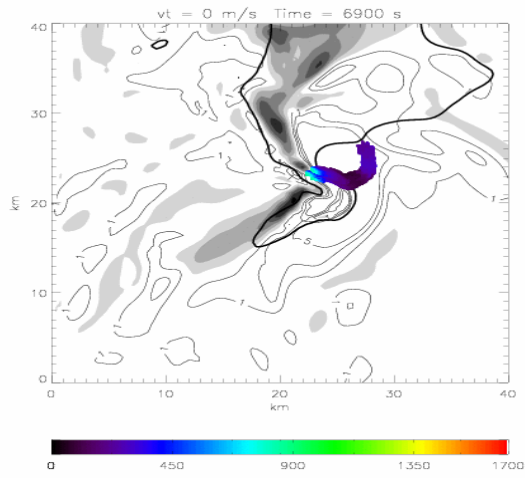
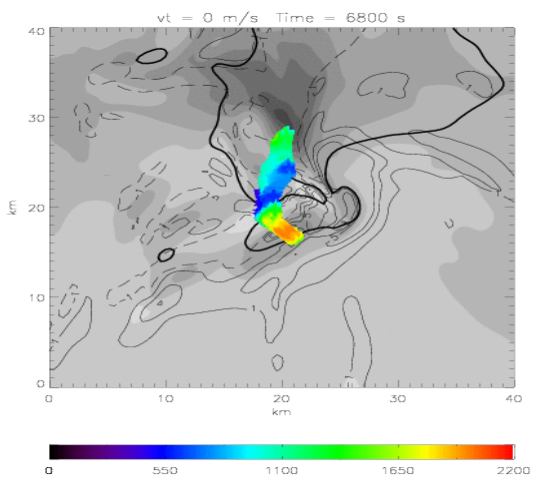
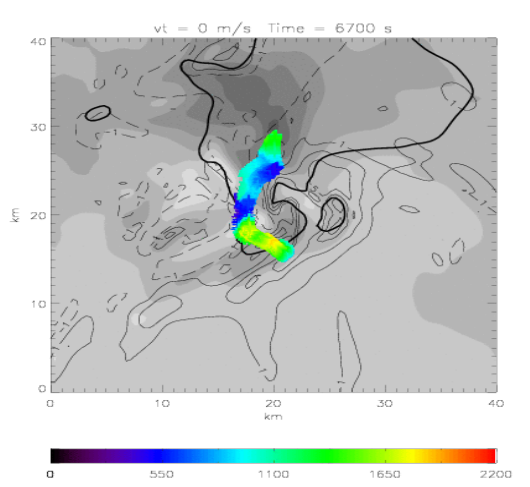
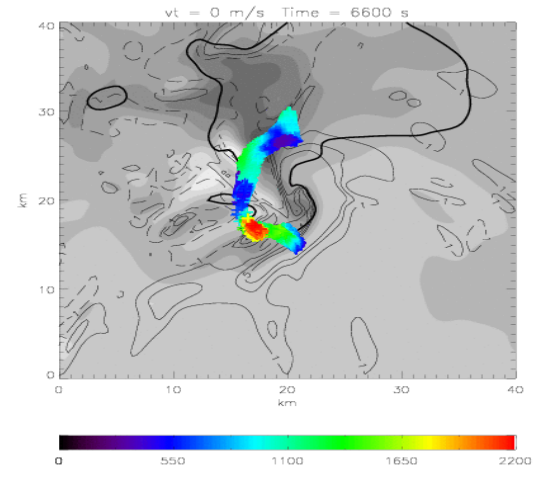
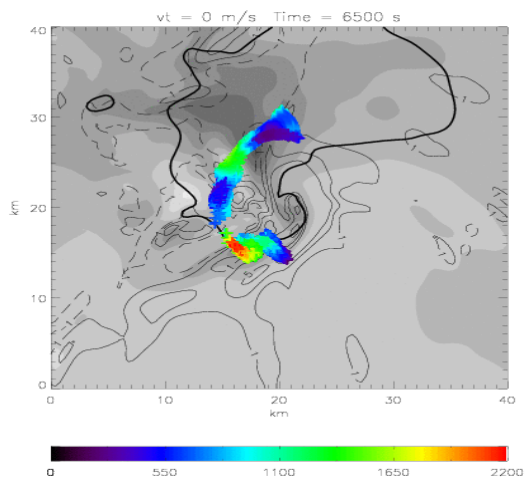
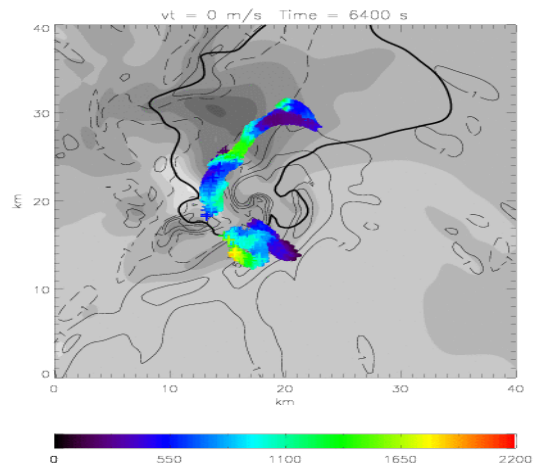
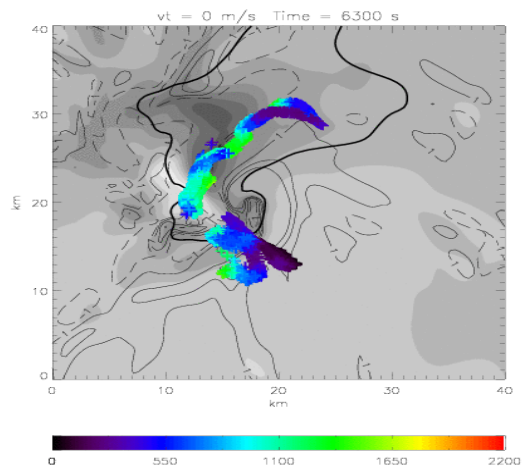


Figure 5: Same as Fig. 4 except particle terminal fall speeds are set to zero.



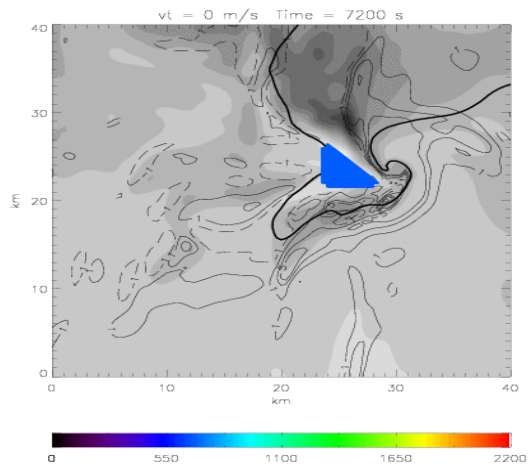
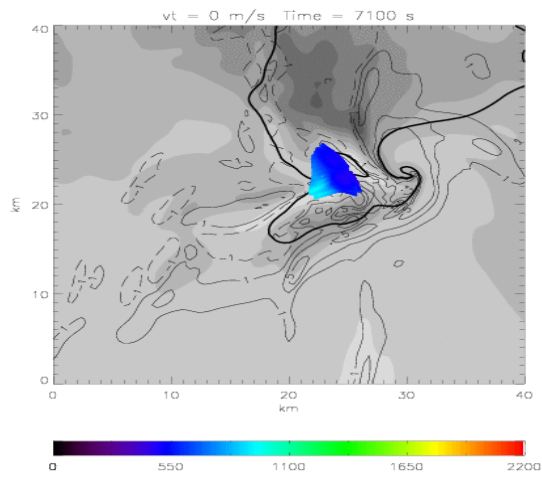
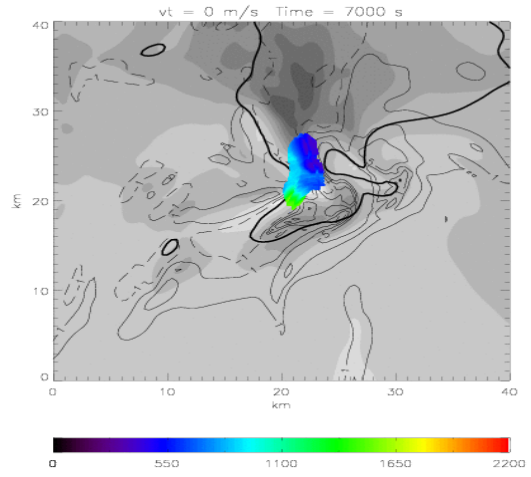
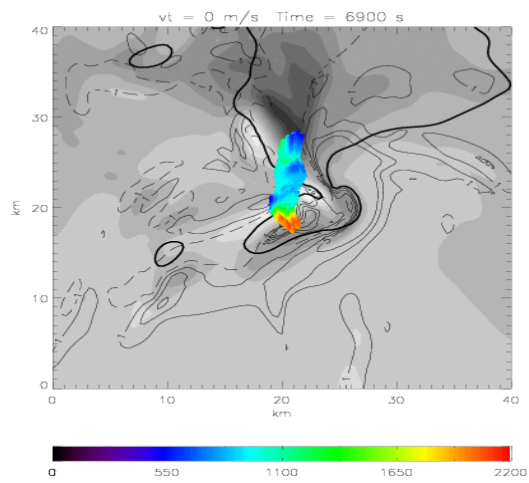


Figure 6: Time series of 5,050 particles initialized as a triangular region in the rear flank downdraft near 700 m. Virtual potential temperature is grey shaded while precipitation is outlined by the thick contour. Downdraft regions are dashed while updraft regions are denoted by thin contours.